

DOCUMENT CONTROL SHEET

	ORIGINATOR'S REF. NLR-TP-2004-319		SECURITY CLASS. Unclassified
ORIGINATOR National Aerospace Laboratory NLR, Amsterdam, The Netherlands			
TITLE Aeroacoustic wind tunnel tests of wind turbine airfoils			
PUBLISHED/PRESENTED Presented at the 10 th AIAA/CEAS Aeroacoustics Conference in Manchester, UK on 10-12 May 2004			
PERMISSION			
AUTHORS S. Oerlemans and Paul Migliore* <small>* National Renewable Energy Laboratory</small>		DATE August 2004	PP 20
REF 17			
DESCRIPTORS microphone array, windturbine noise, trailing edge noise, inflow-turbulence noise			
ABSTRACT <p>Aeroacoustic wind tunnel tests were performed for six airfoils that are candidates for use on small wind turbines. One additional airfoil (NACA 0012) was tested for comparison to benchmark data. The acoustic measurements were performed in NLR's Small Anechoic Wind Tunnel, for a range of wind speeds (U) and angles of attack, with and without boundary layer tripping. Besides the airfoil self-noise measurements in a clean tunnel flow, the models were also tested with a turbulence grid in the nozzle, to investigate airfoil noise associated with inflow turbulence. A 48-microphone out-of-flow acoustic array was used to locate noise sources and to separate airfoil noise from extraneous wind tunnel noise. Special techniques were applied to translate acoustic source plots to absolute airfoil noise spectra. The acoustic results indicate that in a clean tunnel flow trailing edge noise is dominant for all airfoils. In the untripped condition a number of airfoils exhibit intense tones, that disappear after proper tripping is applied. Broadband trailing edge noise levels are found to scale with $U^{4.5}$. The agreement with the benchmark data was generally good. In case of inflow turbulence, leading edge noise is dominant for all airfoils, and no difference is observed between results with and without tripping. The inflow turbulence noise levels are found to scale with U^6. Comparison of the acoustic results for different airfoils indicates that inflow turbulence noise levels increase with increasing sharpness of the model leading edge. The directivity of both trailing edge and inflow turbulence noise is found to be symmetrical with respect to the chord. With regard to the test set-up, it was found that a treatment of porous material at the model-endplate junctions yields a reduction of broadband extraneous noise up to 10 dB. As a result, the array can look much 'deeper', which enables the detection of very low trailing edge noise levels.</p>			



NLR-TP-2004-319

Aeroacoustic wind tunnel tests of wind turbine airfoils

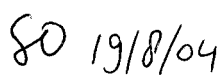
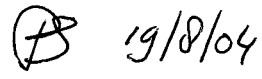
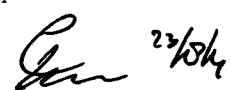
S. Oerlemans and P. Migliore*

* National Renewable Energy Laboratory

This report is based on AIAA paper 2004-3042 presented at the 10th AIAA/CEAS Aeroacoustics Conference in Manchester, UK on 10-12 May 2004.

This report may be cited on condition that full credit is given to NLR and the authors.

Customer: National Aerospace Laboratory NLR
Working Plan number: AV.1.C.1
Owner: National Aerospace Laboratory NLR
Division: Aerospace Vehicles
Distribution: Unlimited
Classification title: Unclassified
August 2004

Approved by author:  19/8/04	Approved by project manager:  19/8/04	Approved by project managing department:  23/8/04
--	--	---



Contents

I. Introduction	3
II. Experimental Method	4
III. Array Processing	5
IV. Trailing Edge Noise	6
V. Inflow Turbulence Noise	9
VI. Conclusion	9
References	10

23 Figures

(20 pages in total)



Aeroacoustic Wind Tunnel Tests of Wind Turbine Airfoils

Stefan Oerlemans*

National Aerospace Laboratory NLR, Emmeloord, The Netherlands

and

Paul Migliore†

National Renewable Energy Laboratory, Golden, Colorado 80401

Aeroacoustic wind tunnel tests were performed for six airfoils that are candidates for use on small wind turbines. One additional airfoil (NACA 0012) was tested for comparison to benchmark data. The acoustic measurements were performed in NLR's Small Anechoic Wind Tunnel, for a range of wind speeds (U) and angles of attack, with and without boundary layer tripping. Besides the airfoil self-noise measurements in a clean tunnel flow, the models were also tested with a turbulence grid in the nozzle, to investigate airfoil noise associated with inflow turbulence. A 48-microphone out-of-flow acoustic array was used to locate noise sources and to separate airfoil noise from extraneous wind tunnel noise. Special techniques were applied to translate acoustic source plots to absolute airfoil noise spectra. The acoustic results indicate that in a clean tunnel flow trailing edge noise is dominant for all airfoils. In the untripped condition a number of airfoils exhibit intense tones, that disappear after proper tripping is applied. Broadband trailing edge noise levels are found to scale with $U^{4.5}$. The agreement with the benchmark data was generally good. In case of inflow turbulence, leading edge noise is dominant for all airfoils, and no difference is observed between results with and without tripping. The inflow turbulence noise levels are found to scale with U^6 . Comparison of the acoustic results for different airfoils indicates that inflow turbulence noise levels increase with increasing sharpness of the model leading edge. The directivity of both trailing edge and inflow turbulence noise is found to be symmetrical with respect to the chord. With regard to the test set-up, it was found that a treatment of porous material at the model-endplate junctions yields a reduction of broadband extraneous noise up to 10 dB. As a result, the array can look much 'deeper', which enables the detection of very low trailing edge noise levels.

I. Introduction

THE U.S. Department of Energy, working through its National Renewable Energy Laboratory (NREL), is engaged in a comprehensive research effort to improve the understanding of wind turbine aeroacoustics. Motivation for this effort is the desire to exploit the large expanse of low-wind-speed sites that tend to be closer to U.S. load centers. NREL's National Wind Technology Center (NWTC) is implementing a multi-faceted approach that includes aerodynamic¹ and acoustic² wind tunnel tests, field tests³ and theoretical analyses⁴.

The present paper describes aeroacoustic wind tunnel tests of six airfoils that are candidates for use on small wind turbines. The tests were conducted in the Small Anechoic Wind Tunnel of the National Aerospace Laboratory (NLR) in the Netherlands. The acoustic measurements were done for a range of wind speeds and angles of attack, and with and without boundary layer tripping in order to assess the effect of blade contamination (due to e.g. dirt or insects) on the noise production. Besides the airfoil self-noise measurements in a clean tunnel flow, the models were also tested with a turbulence grid in the nozzle, to investigate airfoil noise associated with inflow turbulence. A 48-microphone out-of-flow acoustic array was used to locate noise sources and to separate airfoil noise from extraneous

* Research engineer, Aeroacoustics Department, P.O. Box 153, 8300 AD Emmeloord, The Netherlands.

† Research scientist, National Wind Technology Center, 1617 Cole Boulevard, Golden, Colorado.



wind tunnel noise. Special techniques were applied to translate acoustic source plots to absolute airfoil noise spectra. Besides the six candidate airfoils, one airfoil shape (NACA 0012) was acoustically tested for comparison to existing benchmark data from NASA⁵. Prior to the acoustic tests, hotwire measurements were done in the empty test section to determine the turbulence intensity and flow angularity, with and without turbulence grid. The lift characteristics of the different airfoils were measured using a balance.

This paper will focus on the acoustic results. In Section II the experimental method will be described, including the wind tunnel, airfoil models, microphone array, and test program. Section III deals with the array processing techniques that were used to locate and quantify the noise from the airfoils. In Section IV the characteristics of trailing edge noise are presented, while in Section V the inflow turbulence noise results are discussed. Section VI provides the conclusions of the study. In this paper only selected results and overall conclusions will be presented; a more complete and detailed description of the results can be found in Ref. 6.

II. Experimental Method

A. Wind Tunnel

The tests were carried out in NLR's Small Anechoic Wind Tunnel KAT (Figure 1). The KAT is an open circuit wind tunnel, the test section of which is surrounded by a 5x5x3 m³ room which is completely covered with 0.5 m foam wedges, yielding more than 99% absorption above 500 Hz. Two horizontal endplates (0.90 x 0.70 m²) are mounted to the upper and lower sides of the rectangular 0.38 x 0.51 m² nozzle, providing a semi-open test section for airfoil self-noise measurements. To suppress reflections, the endplates are acoustically lined with a 5.5 cm layer of sound absorbing foam covered by a 5% open perforated plate⁷. In case of inflow turbulence measurements, a turbulence grid is installed in the nozzle. The turbulence grid consists of diagonally oriented, cylindrical 12 mm bars with a mesh width of 60 mm.

Due to the open jet set-up, the effective angle of attack will be smaller than the geometrical angle of attack. The magnitude of this 'open jet effect' depends on the dimensions of the wind tunnel and the model chord. Here, the effective angle of attack was calculated according to Ref. 5, which implies that for the KAT the geometrical angle of attack is divided by 2.26.

Prior to the acoustic tests, the flow quality in the empty test section was verified by hot-wire measurements. Without the turbulence grid, the turbulence intensities in the central part of the test section were less than 1%. With the turbulence grid installed, the local turbulence levels increased to about 11% and 6% at locations corresponding to the model leading and trailing edges respectively. Although the flow angularity increased slightly with increasing speed and turbulence level, it always remained within 1° in the central area of the test section. The axial and lateral turbulence spectra showed broadband turbulence without spectral peaks.

B. Airfoil Models

The airfoil models had a chord of 0.23 m and a span of 0.51 m. The models were built to exacting tolerances, where the difference between specified and as-built coordinates was within 0.12 mm in virtually every case. The trailing edge thickness was less than 0.23 mm to prevent blunt trailing edge noise. The shape of the airfoils is given in Figure 2. In addition to the six candidate airfoils, a NACA 0012 airfoil was tested for comparison to benchmark data. Tripping of the models was done using zigzag tape of 11 mm width over the complete span, at 2% chord and 5% chord on the suction and pressure sides of the airfoil respectively. The standard trip thickness was 0.25 mm, but for a number of conditions, trips of up to 0.5 mm were used.

C. Microphone Array

The microphone array, which consisted of 48 ½-inch microphones (type LinearX M51) mounted in an open grid (Figure 1), was designed for maximum side-lobe suppression at frequencies between 1 and 20 kHz⁸. To obtain high resolution at low frequencies, the array dimensions needed to be rather large (0.8 x 0.6 m²). The array was placed outside the tunnel flow at a distance of 0.6 m from the tunnel axis, on either the suction or pressure side of the model. This relatively small distance between the array and the model was chosen to obtain maximum signal-to-noise ratio and high resolution at low frequencies. The center of the array was placed at the same height as the tunnel axis.

Acoustic data from the microphones were synchronously measured at a sample frequency of 51.2 kHz and a measurement time of 30 s. A 500 Hz high-pass filter was used to enhance the dynamic range. The acoustic data were processed using a block size of 2048 with a Hanning window and an overlap of 50%, yielding 1500 averages and a



narrowband frequency resolution of 25 Hz. The frequency response of the individual array microphones was taken from calibration sheets.

D. Test Program

Array measurements were mainly done on the suction side of the six candidate airfoils, with and without tripping and with and without turbulence grid, for three angles of attack and Reynolds numbers between 0.35 and 1 million. The NACA 0012 airfoil was tested for the same conditions as in Ref. 5, i.e. with and without trip, without turbulence grid, for four Reynolds numbers (from 0.5 to 1.12 million) and five angles of attack. For a number of conditions, pressure side array measurements were done as well, to determine directivity effects. Some measurements were repeated with thicker trips to assess their effectiveness.

III. Array Processing

A. Source Localization

Conventional beamforming⁹ was used to obtain acoustic source plots in 1/3-octave bands. To improve the resolution and further suppress background noise from the tunnel, the main diagonal in the cross power matrix (autopowers) was discarded (see also Ref. 10). The effect of sound refraction by the tunnel shear layer was corrected using the Amiet method¹¹. The array scan plane was placed in the plane of the model and rotated in accordance with the angle of attack. The scan resolution was 0.5 cm in both directions and the scan levels were normalized to a distance of 0.282 m $[(4\pi)^{-1/2}]$, so that for a monopole source the peak level in the source plot corresponds to the Sound Power Level.

Typical examples of acoustic source plots for airfoil measurements without and with inflow turbulence are given in Figure 3 and Figure 4 respectively. These acoustic source plots show the distribution of the noise sources in the plane of the model as a function of frequency. The tunnel flow goes from left to right and the airfoil contour is indicated by the gray line. The levels in these plots are Sound Power Levels in dB's (1/3 octave band levels), and the dynamic range of the color scale is always 12 dB. Note that the level of the color scale is adjusted to the maximum level in the plot, so that the same colors do not necessarily correspond to the same levels for different plots. These figures illustrate that without inflow turbulence the noise is radiated from the trailing edge, while *with* turbulence the (dominant) noise source is located at the model leading edge. This shift of the dominant noise source region from trailing- to leading edge after introducing inflow turbulence was observed for practically all measurements, and can be explained by the different mechanisms responsible for inflow turbulence and trailing edge noise¹². Besides noise from the airfoil, for some conditions extraneous noise sources can be observed as well. An example of extraneous sources are the high levels at $x=0$ for 2.5 and 3.15 kHz in Figure 4, which originate from the turbulence grid in the nozzle. Note that the peak levels in Figure 4 do not exactly coincide with the model leading edge. This is probably due to the fact that the deflection of the open jet is not taken into account in the array processing. However, through the use of an integration contour (see next section), the peak is captured anyway.

B. Airfoil Noise Spectra

The acoustic source plots were further processed to obtain absolute airfoil noise levels. A schematic representation of the 'power integration' procedure is shown in Figure 5 (note that similar methods are described in Refs. 13 and 14). The method used here is similar to the method described in Ref. 10, but a number of additional measures were taken to reduce effects of coherence loss. To prevent tunnel background noise from obscuring the calculated airfoil noise levels^{10,13}, the main diagonal of the cross power matrix was discarded. In addition, a spatial window was applied to the microphone signals, which corrects for the variation in microphone density over the surface of the array, and which reduces the effective array aperture with increasing frequency.

Rather than using the peak level at the mid-span position in the acoustic source plot (as in Refs. 10 and 13), an integration contour was used (see Figure 5). The reason for this is that in the presence of coherence loss, peaks in the source plots tend to 'smear out', resulting in reduced peak levels. By using an integration contour this effect is suppressed. By choosing an integration contour around the mid-span part of the model, the influence of extraneous sources at model-endplate junctions (see e.g. left plot in Figure 5) is suppressed. For measurements with a clean tunnel flow, a trailing edge integration was used. For measurements with inflow turbulence, a leading edge contour was used. To obtain absolute airfoil noise levels, the source plot levels within the integration contour were summed and multiplied by an Array Calibration Function (ACF) determined from simulations of an uncorrelated line source¹⁰. To overcome possible problems due to the removal of the main diagonal of the cross power matrix¹⁴,



negative source powers in the acoustic source plot were discarded in the summation. The resulting acoustic spectra give the Sound Power Level of the airfoil noise produced by 10 cm of span in 1/3-octave bands.

The power integration procedure was validated by comparing the array-determined trailing edge noise spectra to the absolute sound levels at the central array microphone. Because the single microphone levels were sometimes dominated by tunnel background noise, one of the noisiest trailing edge noise cases was chosen. As shown in Figure 6, the agreement between the array-determined spectrum and the single-microphone levels is very good. For high frequencies, comparison is not possible because the single-microphone levels are dominated by tunnel background noise.

C. Extraneous Sources

In a number of cases the airfoil noise levels were so low that, despite the procedures described above, the airfoil noise spectra were dominated by extraneous tunnel noise sources. In order to allow fast judgment of the validity of the measured levels, procedures were developed to indicate the importance of tunnel noise in the spectra. The trailing edge noise levels could be influenced by extraneous sources at the model-endplate junctions ('corner sources', see e.g. left plot in Figure 5). Therefore, a routine was used which determines the importance of these corner sources and which, in case the influence of the corner sources on the trailing edge noise level is more than 1 dB, calculates an upper limit for the 2D trailing edge noise level (Figure 7). This routine was developed by performing simulations of an uncorrelated line source with extraneous corner sources of varying strengths. In the trailing edge noise spectra the upper limits are indicated by the absence of a marker at that specific frequency. If no (important) corner sources are found, this is indicated in the spectrum by a marker. Note that in Section IV-F a method is described to physically reduce these corner sources.

For the grid measurements, rather than corner sources, background noise from the turbulence grid itself dominated the leading edge noise levels in a number of cases (Figure 4). Therefore, for these measurements the leading edge noise levels from the measurement *with* model were compared to the levels obtained in the empty test section (with turbulence grid) for the same speed. In case the leading edge noise level with model is more than 6 dB higher than the background noise level, this is indicated by a marker in the spectrum. Thus, the absence of a marker indicates that the spectral level can be influenced by grid noise. Note that due to the removal of the main diagonal of the cross power matrix, a dominant grid noise source may also give a negative contribution to the level at the leading edge position, for some frequencies.

IV. Trailing Edge Noise

In this section the trailing edge noise results will be presented. First, the general characteristics will be discussed, such as dependence on speed and angle of attack. Then, some subjects will be discussed in more detail, such as the occurrence of tones, comparison to benchmark data, and the comparison of trailing edge noise from different airfoils. Finally, a method to physically reduce extraneous noise sources will be discussed. For reasons of conciseness, the results will focus on two airfoils, i.e. the NACA 0012 and the S834, and only two angles of attack.

A. General Characteristics

Trailing edge noise spectra for the NACA0012 and S834 airfoils are given in Figure 8 and Figure 9 respectively. Results are shown for various wind speeds, two angles of attack, and with and without trip. As explained in Section III-B, the absence of a marker at a specific frequency indicates that the plotted level is an upper limit for the actual 2D trailing edge noise level. Both airfoils show a clear difference between tripped and untripped data. Whereas the tripped results exhibit smooth, broadband spectra, which can be associated with turbulent-boundary-layer-trailing-edge noise, the untripped results show significant peaks for most speeds and angles of attack. As a result of the thin trailing edge of the models, these tones cannot be explained by trailing edge bluntness vortex shedding noise. They can be associated, however, with laminar boundary layer vortex shedding⁵. This mechanism involves a feedback loop between noise from the trailing edge and Tollmien-Schlichting instability waves originating at an upstream location in the laminar boundary layer. The frequency of these peaks can be seen to increase with speed, while the intensity increases with angle of attack.

The speed dependence of the trailing edge noise spectra was investigated in more detail by plotting normalized levels as a function of the Strouhal number $St=fC/U$, where f is frequency, C is model chord, and U is wind speed. The normalized levels were calculated as $PWL-10\log_{10}(U^m)$, where PWL is the airfoil Sound Power Level determined from the array measurements (see Section III-B) and m denotes the speed dependence of the airfoil noise levels. The optimum value for m was found to be 4.5. The resulting normalized spectra for both airfoils are shown in Figure 10 and Figure 11. It can be seen that a very good data collapse is obtained for the tripped conditions: for a



given angle of attack, the trailing edge noise levels at different speeds coincide within 1-2 dB. The optimum value of $m = 4.5$ is slightly lower than the value of 5 found in Ref. 5. A reason for this discrepancy could be that, despite several measures that were taken to reduce coherence loss (see Section III-B), this effect still plays a role, resulting in lower levels at high wind speeds. On the other hand, several studies of slat noise^{15,16}, which may be regarded as a trailing edge noise mechanism, also find a value of 4.5. This could indicate that the value of 4.5 is real.

For untripped conditions, the vortex shedding tones in Figure 10 and Figure 11 do not collapse very well. Although the peak Strouhal numbers for different speeds coincide within about 30%, the normalized peak levels differ significantly. Other values of m did not significantly improve the collapse. This illustrates that the normalization described above does not work very well for the complex feedback mechanism associated with laminar-boundary-layer-vortex-shedding noise. The slight increase in peak Strouhal numbers with speed (for a given angle of attack) suggests that a better collapse of peak frequencies might be obtained if the boundary layer thickness (rather than chord) is used as the length scale in St (as in Ref. 5), as the boundary layer thickness at the trailing edge decreases with increasing Reynolds number. It is noted that the trends observed here are very similar to those in Ref. 5.

B. Tones and Effect of Tripping

Three of the six airfoils showed intense, narrowband tones in the trailing edge noise spectra for the untripped condition. Here only the S834 tones will be discussed in more detail. As discussed in the previous section, these tones can be attributed to laminar-boundary-layer-vortex-shedding-noise. The tones were most prominent at 22 m/s and $\alpha=10^\circ$, where they occur around 1 and 2 kHz (see Figure 9). The corresponding acoustic source plots are shown in Figure 12. Note that the spanwise extent of the source region is smaller than for the broadband trailing edge noise in Figure 3. This suggests that the feedback loop responsible for the spectral peaks is interrupted close to the endplates.

The sensitivity of the tones to trip thickness is illustrated in Figure 13, which shows the narrowband spectra of the S834 airfoil as a function of trip thickness. It can be seen that the standard trip thickness of 0.25 mm on both sides is not effective: the level of the 925 and 1850 Hz tones even increases slightly with respect to the untripped case, and an extra harmonic at 2775 Hz appears. After application of a slightly thicker trip (0.30 mm) on the pressure side only, the spectral levels decrease dramatically and the 925 and 1850 Hz tones vanish completely (although a less intense peak at 2775 Hz remains). Interestingly, the broadband level decreases even further after the addition of a 0.3 mm trip on the suction side. This suggests that for the S834 airfoil the suction side boundary layer dominates broadband noise production, whereas the pressure side may generate tones if it is not properly tripped. The tones were also found to disappear in case of inflow turbulence (not shown), which apparently interrupts the feedback mechanism as well.

C. Directivity

To assess the directivity of the radiated noise, in addition to the suction side array measurements, tests were also done with the array on the pressure side. Because the array position was fixed (on either suction or pressure side), the measured direction varies with the model angle of attack (see Figure 14). The noise radiation in both directions is compared for the NACA 0012 and S834 airfoils in Figure 15. This figure shows that the noise spectra on both sides are practically identical. For zero angle of attack, the difference is less than one dB. For the higher angle of attack, the suction side levels can be seen to be slightly higher than the pressure side levels. This small difference can be understood from the $\sin^2(\theta/2)$ directivity of trailing edge noise¹³. In conclusion, the results indicate a symmetric directivity with respect to the chord.

D. Comparison to Benchmark Data

Acoustic measurements were done on the NACA 0012 airfoil, in order to enable direct comparison to existing benchmark data from NASA (Ref. 5). The airfoil shape and chord were identical, and in both studies the 2D model was mounted between two endplates attached to opposite sides of the rectangular tunnel nozzle. The NLR nozzle ($0.38 \times 0.51 \text{ m}^2$) was somewhat larger than NASA's ($0.31 \times 0.46 \text{ m}^2$), resulting in a larger model span for the NLR tests (0.51 m versus 0.46 m). Whereas in the present tests tripping was done using 0.25 mm zigzag tape at 2% (suction side) and 5% (pressure side) chord, NASA employed a random distribution of grit in strips from the leading edge to 20 % chord. The NLR measurements were done at the same tunnel speeds and effective angles of attack as in the NASA study.

In the present tests, acoustic data were acquired with a 48-microphone phased array, and trailing edge noise spectra were determined by integrating the mid-span trailing edge area in the acoustic source plots (see Section III-B). In the NASA tests, cross-correlations between pairs of microphones were used to separate trailing



edge noise from other sources. In order to account for the differences in level definition, in the present paper 6.14 dB has been added to the NASA levels. No correction was made for differences in directivity. The NASA data represent noise levels as perceived at $\theta=90^\circ$, whereas the NLR levels are determined by the average radiation in the direction of the array.

A representative example of the comparison between the NASA and NLR data is presented in Figure 16. It can be seen that the general character of the spectra is well reproduced, i.e. broadband spectra for the tripped cases and spectral humps or tones for untripped cases at nonzero angle of attack. The frequencies of these humps correspond quite well, although differences in level occur, probably due the sensitivity of the source mechanism to small geometric details. The tripped results reveal an interesting difference between the NASA and NLR data: although the spectral levels correspond quite well for intermediate frequencies (2-4 kHz), the NASA data show a dominant hump around 1 kHz with a 'shoulder' around 3 kHz. The 1 kHz hump does not appear in the NLR data.

The NASA data⁵ show the low-frequency hump for most speeds and angles of attack, and also for models with a different chord. The peak frequency of the hump seems to increase with decreasing chord, increasing speed, and decreasing angle of attack. The speed dependence of the peak frequency does not appear to be linear. In the NASA study the measured spectra are compared to predictions that include several airfoil self-noise mechanisms. For higher angles of attack, a double hump in the spectrum is explained by (1) a different contribution from the suction- and pressure side boundary layer, each with its own peak frequency, and (2) separation of the suction side boundary layer. However, this does not explain the double hump (i.e. the 1 kHz hump and the 'shoulder' around 3 kHz) in the spectrum at $\alpha=0^\circ$: at zero angle of attack the pressure- and suction-side boundary layers should be identical for the symmetrical NACA 0012 airfoil, so that the noise spectrum should only have a single hump. A possible cause for the 1 kHz hump in the NASA data could be the presence of extraneous noise sources at the junctions between the endplates and the model trailing edge in the NASA tests (their two-microphone source location method does not allow distinction between corner sources and sources along the span). However, from experience in other tests and with different methods, corner sources are not considered to be present in the NASA results¹⁷. An alternative explanation for the double humps could be reflections or multi-path type effects from the endplate corner region¹⁷.

In conclusion, although the general agreement between NASA and NLR results is quite good, no satisfactory explanation was found for the discrepancy for the tripped results at 1 kHz. A remaining possibility is the difference in trip method: the NASA trips, consisting of a random distribution of grit in strips from the leading edge to 20% chord, were probably more severe than the 0.25 mm zigzag tapes employed by NLR. This may have caused a difference in boundary layer development and consequently in the radiated noise.

E. Comparison of Different Airfoils

Although the different models were tested for different speed and angle of attack ranges, all airfoils were tested at a speed of 32 m/s and $\alpha=0^\circ$ and 10° (9.5° for the NACA0012 airfoil). This enables a direct comparison of the acoustic results for identical conditions, so that the influence of airfoil shape on trailing edge noise can be assessed. However, comparison at the same angle of attack implies that the aerodynamic performance may be different¹.

The trailing edge noise spectra for the different airfoils are shown in Figure 17 (note that the scales on the y -axis are different). It can be seen that without tripping most airfoils exhibit tones, and significant differences between the airfoils are observed. For zero angle of attack, the symmetrical NACA 0012 airfoil is quietest, while at 10° it is noisiest. The SD2030 shows the opposite behavior. Even the rather similar S822 and S834 show differences of more than 10 dB, illustrating the sensitivity of the noise production to small details. After application of proper tripping, the noise levels are generally much lower due to the elimination of the laminar-boundary-layer-vortex-shedding tones. As a result, the differences between the airfoils are smaller as well. Still, significant differences can be observed between the airfoils. For example, at higher frequencies the NACA 0012 is noisiest, while at lower frequencies it is quieter than the S822 and S834. In the future these observations may be used for validation of trailing edge noise prediction codes that take airfoil shape into account.

F. Reduction of Extraneous Noise Sources

At the end of the test program, it was attempted to physically suppress the extraneous noise sources at the model-endplate junctions ('corner sources', see Section III-C). In the standard set-up, small gaps were present between the model and the endplates, in order to enable balance measurements. Several corner noise reduction techniques were tested, including closing the gaps with tape, applying a single serration at the trailing edge corners, and smoothing the corners with plasticine. Some of these devices were successful at some frequencies, but gave an increase of the extraneous noise sources at other frequencies. Finally, a treatment consisting of filling the gaps with porous foam and closing the last 10-20% chord with tape was applied. This treatment resulted in a drastic broadband reduction of



the corner sources (see Figure 18, note the different color scales). It can be seen that broadband reductions of up to 10 dB are achieved, which enables the detection of very low trailing edge noise levels.

V. Inflow Turbulence Noise

Besides the trailing edge noise measurements in a clean tunnel flow, the models were also tested with a turbulence grid in the nozzle, to investigate leading edge noise associated with inflow turbulence (Figure 4). In general the measured inflow turbulence noise levels are much higher than the trailing edge noise levels. This does not imply that in practice inflow turbulence noise will be dominant for these airfoils. On a real wind turbine, the inflow turbulence levels depend on the (atmospheric) turbulence levels in the incoming flow, which may be much lower than the turbulence intensities produced by the grid in the wind tunnel (about 11%, see Section II-A). As a result, trailing edge noise will be dominant for most wind turbines. Therefore, the grid measurements in the present test should be regarded as a study into the susceptibility of the different airfoils to inflow turbulence noise, for a given level of turbulence in the incoming flow.

In this section first the general characteristics of inflow turbulence noise will be discussed, such as dependence on speed and angle of attack. Then directivity is discussed, followed by a comparison of the noise from different airfoils. For reasons of conciseness, the results will focus on the S822 airfoil, for two angles of attack.

A. General Characteristics

Inflow turbulence noise spectra for the S822 airfoil are given in Figure 19. Results are shown for various wind speeds, two angles of attack, and with and without trip. As explained in Section III-B, the absence of a marker at a specific frequency indicates that the plotted level may be influenced by grid noise. It can be seen that the tripped results are practically identical to the untripped results. No tones are observed, which is line with the broadband character of the grid turbulence (see Section II-A).

Similar to the trailing edge noise results, the speed dependence of the inflow turbulence noise spectra was investigated in more detail by plotting normalized levels as a function of the Strouhal number. The normalized levels are again calculated as $PWL-10 \cdot \log_{10}(U^m)$, where m denotes the speed dependence of the airfoil noise levels. The optimum value for m was found to be 6. The resulting normalized spectra for both angles of attack are shown in Figure 20. It can be seen that a very good data collapse is obtained: the inflow turbulence noise levels at different speeds coincide within a few dB, except the levels which are influenced by grid noise (without marker). The optimum value of $m=6$ is in good agreement with theoretical predictions for low-frequency inflow turbulence noise¹². The dependence of the inflow turbulence noise spectra on angle of attack is shown in Figure 21 for two airfoils. These plots clearly show a noise increase at high frequencies for high angles of attack.

B. Directivity

The directivity of the inflow turbulence noise was measured in the same way as for the trailing edge noise (see Section IV-C). The noise spectra on pressure and suction side are compared in Figure 22 for the S822 airfoil. Similar to the trailing edge noise results, at zero angle of attack the spectra are practically identical. For the higher angle of attack some differences are observed. The fact that at low frequencies the pressure side levels are higher than on the suction side can be understood from the $\sin^2(\theta/2)$ directivity as discussed in Section IV-C (in this case with respect to the model *leading* edge). At higher frequencies the pressure side levels drop below the suction side levels. This is believed to be due to a negative contribution from the grid noise to the level at the leading edge position (see also Section III-C). In conclusion, the results indicate a symmetric directivity with respect to the chord.

C. Comparison of Different Airfoils

Inflow turbulence noise spectra for the different airfoils are compared in Figure 23. Because the leading edge noise spectra are practically identical for tripped and untripped conditions (see previous section), only tripped results are shown here. Clear differences between noise levels, of up to more than 5 dB, can be observed. Note that for some airfoils the levels are less than 6 dB above the empty tunnel levels, so that no marker is shown. By comparing these results with the airfoil shapes in Figure 2, a clear trend can be identified: the sharper the airfoil leading edge, the higher the inflow turbulence noise levels.

VI. Conclusion

Aeroacoustic wind tunnel tests were performed for six airfoils that are candidates for use on small wind turbines. A microphone array was used to locate and quantify leading- and trailing edge noise from the airfoils. The method used to quantify the array results was successfully validated by comparison to single-microphone levels. In a clean



tunnel flow trailing edge noise is dominant for all airfoils. In the untripped condition, a number of airfoils exhibit intense tones that disappear after proper tripping is applied. The broadband sound levels are found to scale with $U^{4.5}$. In case of inflow turbulence, leading edge noise is dominant for all airfoils and no difference is observed between the results with and without tripping. The inflow turbulence noise levels are found to scale with U^6 . Comparison of the acoustic results for different airfoils indicates that inflow turbulence noise levels increase with increasing sharpness of the model leading edge. The directivity of both trailing edge and inflow turbulence noise is found to be symmetrical with respect to the chord. Comparison with benchmark data generally shows good agreement in terms of spectral shape and levels. For the tripped condition, however, a discrepancy at low frequencies is observed, for which no clear explanation was found. With regard to the test set-up, it was found that a treatment of porous material at the model-endplate junctions yielded a broadband extraneous noise reduction of up to 10 dB. As a result, the array can look much 'deeper', which enables the detection of very low trailing edge noise levels.

References

- ¹ Selig, M.S., and McGranahan, B.D., "Wind Tunnel Aerodynamic Tests of Six Airfoils for Use on Small Wind Turbines", AIAA paper 2004-1188, January 2004.
- ² Migliore, P., and Oerlemans, S., "Wind Tunnel Aeroacoustic Tests of Six Airfoils for Use on Small Wind Turbines", AIAA paper 2004-1186, January 2004.
- ³ Migliore, P., van Dam, J., and Huskey, A., "Acoustic Tests of Small Wind Turbines", AIAA paper 2004-1185, January 2004.
- ⁴ Moriarty, P., "Development and Validation of a Semi-Empirical Wind turbine Aeroacoustic Code", AIAA paper 2004-1189, January 2004.
- ⁵ Brooks, T.F., Pope, D.S., and Marcolini, M.A., "Airfoil Self-Noise and Prediction", NASA Reference Publication 1218, 1989.
- ⁶ Oerlemans, S., "Wind tunnel Aeroacoustic Tests of Six Airfoils for Use on Small Wind Turbines, NREL report SR-500-34470, April 2004.
- ⁷ Oerlemans, S., and Sijtsma, P., "Effects of Wind Tunnel Side-Plates on Airframe Noise Measurements with Phased Arrays", AIAA paper 2000-1938, June 2000.
- ⁸ Sijtsma, P., and Holthusen, H., "Source Location by Phased Array Measurements in Closed Wind Tunnel Test Sections", AIAA paper 1999-1814, May 1999.
- ⁹ Johnson, D.H., and Dudgeon, D.E., "Array Signal Processing", Prentice Hall, 1993.
- ¹⁰ Oerlemans, S., and Sijtsma, P., "Determination of Absolute Levels from Phased Array Measurements Using Spatial Source Coherence", AIAA paper 2002-2464, June 2002.
- ¹¹ Amiet, R.K., "Refraction of Sound by a Shear Layer", Journal of Sound and Vibration, Vol. 58, No. 2, pp. 467-482, 1978.
- ¹² Blake, W.K., "Mechanics of Flow-Induced Sound and Vibration", Academic Press, 1986.
- ¹³ Hutcheson, F.V., and Brooks, T.F., "Effects of Angle of Attack and Velocity on Trailing Edge Noise", AIAA paper 2004-1031, January 2004.
- ¹⁴ Brooks, T.F., and Humphreys, W.M., "Effect of Directional Array Size on the Measurement of Airframe Noise Components", AIAA paper 1999-1958, May 1999.
- ¹⁵ Pott-Pollenske, M., Dobrzynski, W., Buchholz, H., Gehlar, B., and Walle, F., "Validation of a Semiempirical Airframe Noise Prediction Method through Dedicated A319 Flyover Noise Measurements", AIAA paper 2002-2470, June 2002.
- ¹⁶ Pott-Pollenske, M., Alvarez-Gonzalez, J., and Dobrzynski, W., "Effect of Slat Gap on Farfield Radiated Noise and Correlation with Local Flow Characteristics", AIAA paper 2003-3228, May 2003.
- ¹⁷ Personal communication with T.F. Brooks, 2003.



Figures



Figure 1: Wind tunnel set-up with lined endplates, airfoil model (in white), and microphone array. Flow goes from left to right.

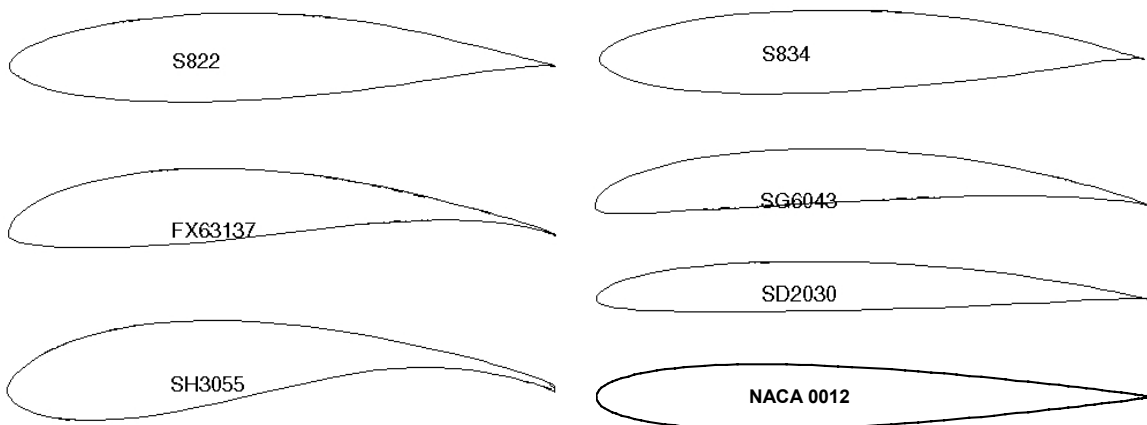


Figure 2: Overview of tested airfoil shapes.

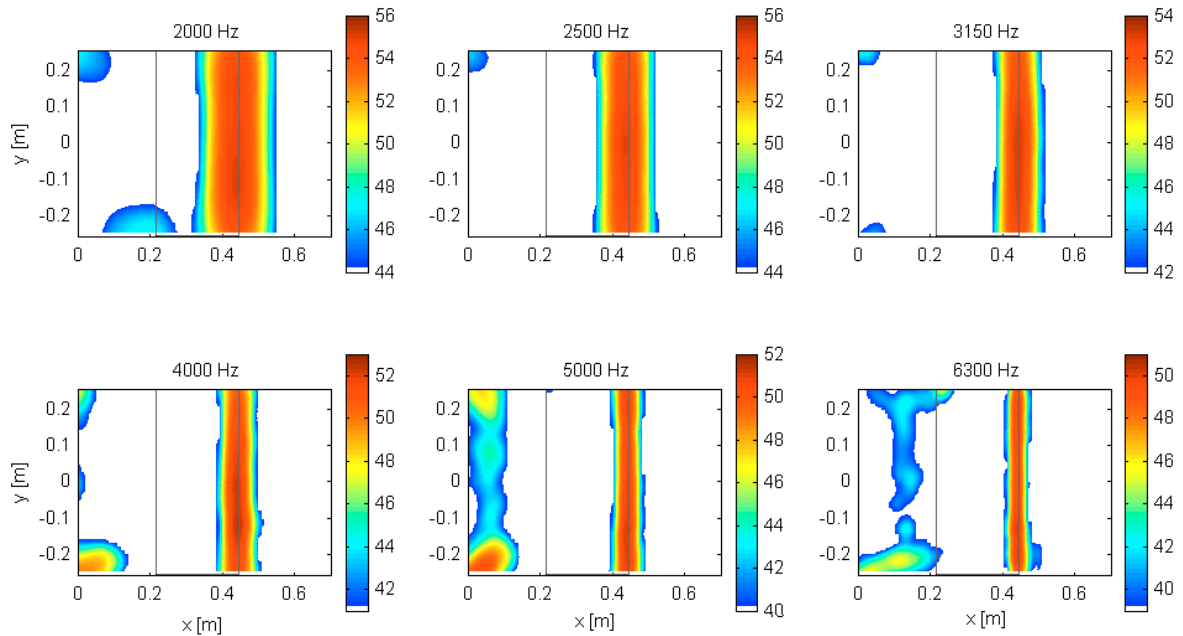


Figure 3: Typical acoustic source plots for an airfoil in clean tunnel flow, showing broadband trailing edge noise. These plots show the distribution of noise sources in the plane of the model as a function of frequency. The model contour is indicated by the black line, and flow goes from left to right. The maximum of the color scale is adjusted to the maximum in the plot, and the dynamic range is always 12 dB.

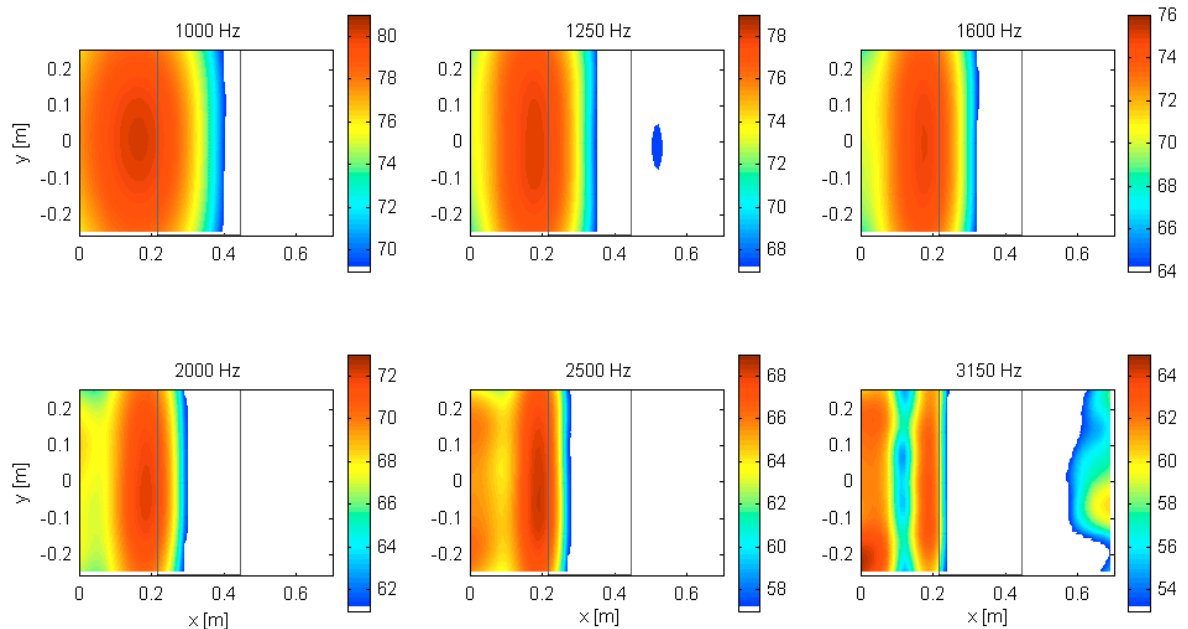


Figure 4: Typical acoustic source plots for an airfoil in turbulent tunnel flow, showing broadband leading edge noise. These plots show the distribution of noise sources in the plane of the model as a function of frequency. The model contour is indicated by the black line, and flow goes from left to right. The maximum of the color scale is adjusted to the maximum in the plot, and the dynamic range is always 12 dB. The noise radiated from $x=0$ at high frequencies is due to the turbulence grid in the tunnel nozzle.

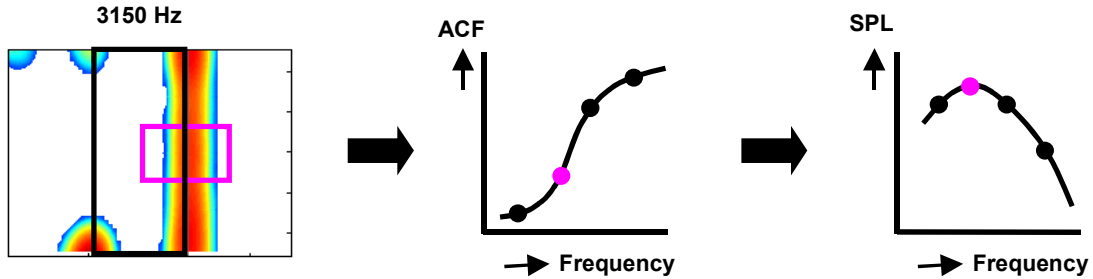


Figure 5: Schematic representation of the power integration method used to quantify trailing edge noise. The source plot levels within the pink contour (left) are summed and multiplied by the frequency-dependent Array Calibration Function (middle) to obtain the trailing edge noise spectrum (right). By using an integration contour, the trailing edge noise is separated from extraneous sources at the model-endplate junctions. For measurements with inflow turbulence a leading edge integration contour was used.

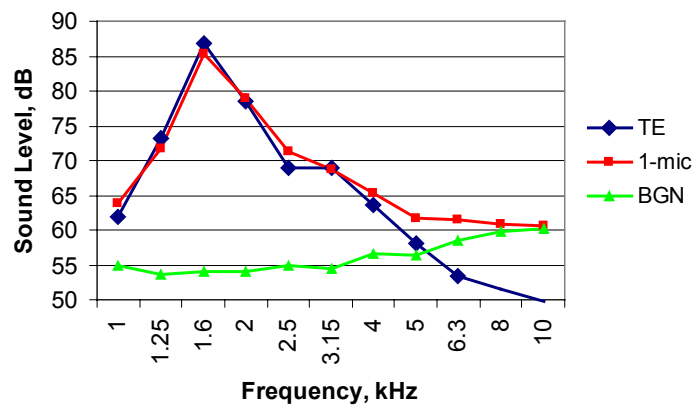


Figure 6: Validation of the power integration method. 'TE' is the trailing edge noise spectrum as determined from the acoustic source plots (see Figure 5), '1-mic' is the sound pressure level at the central array microphone, and 'BGN' is the background noise spectrum. It can be seen that the agreement between TE and 1-mic is good. For high frequencies the single-microphone spectrum is dominated by background noise.

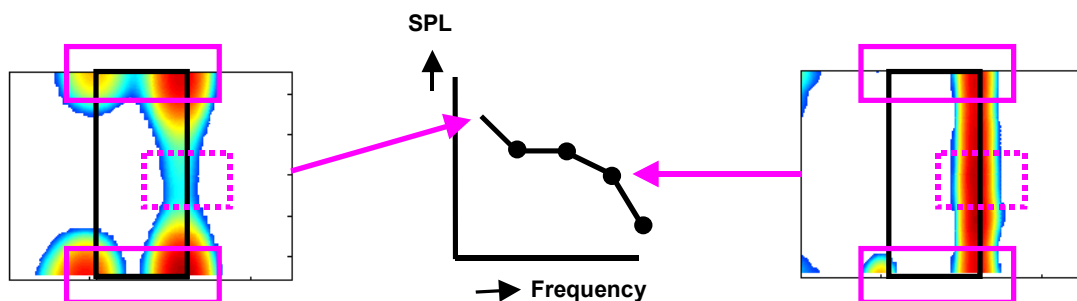


Figure 7: Schematic representation of the method used to account for extraneous noise sources at the model-endplate junctions. The extraneous source levels within the pink contours are summed and compared to the trailing edge noise level (dotted contour). If the influence of extraneous sources on the trailing edge noise level is significant (i.e. more than 1 dB, see left plot), an upper limit for the actual trailing edge noise level is calculated. This is indicated in the trailing edge noise spectrum by the absence of a marker (see middle plot). If the influence of extraneous sources is negligible (right plot), a marker is plotted in the spectrum.

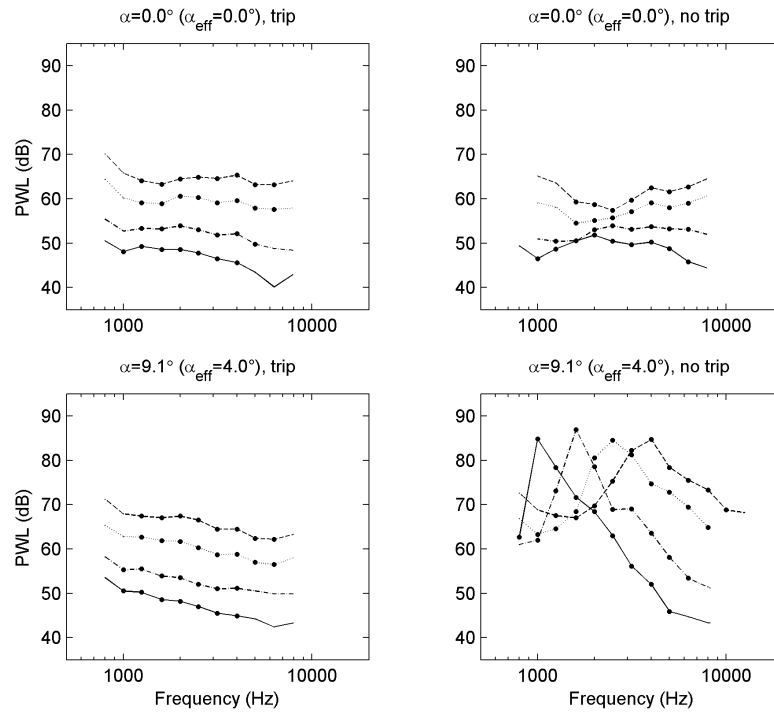


Figure 8: Trailing edge noise spectra for NACA0012 airfoil: __ 32 m/s; _ 40 m/s; ... 56 m/s; __ 71 m/s.

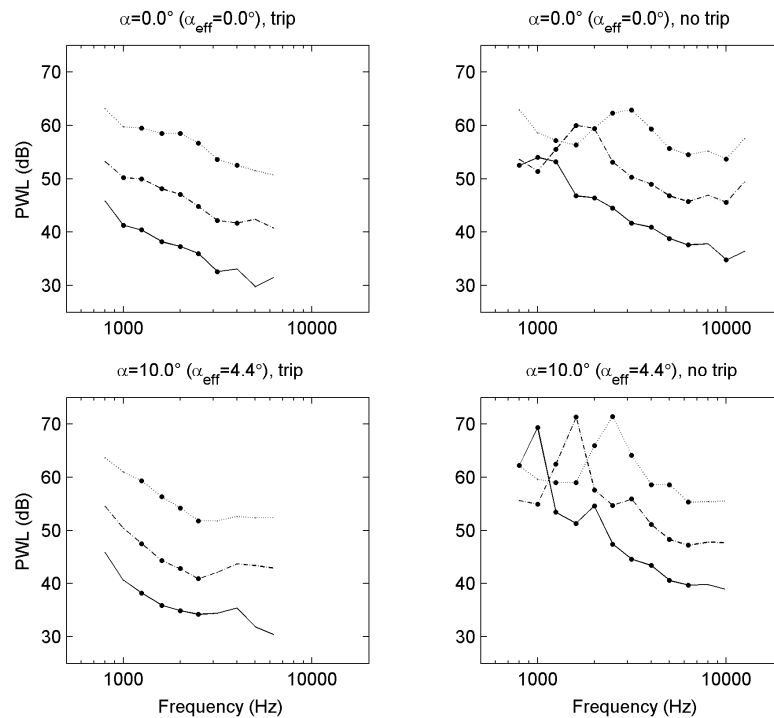


Figure 9: Trailing edge noise spectra for S834 airfoil: __ 22 m/s; _ 32 m/s; ... 48 m/s.

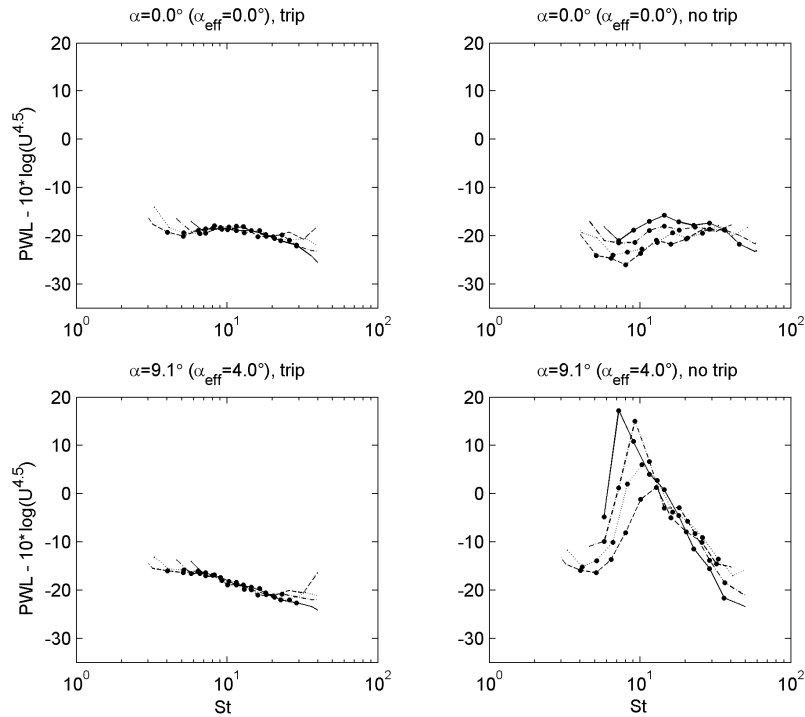


Figure 10: Normalized trailing edge noise spectra for NACA0012 airfoil (compare to Figure 8): __ 32 m/s; _ _ 40 m/s; ... 56 m/s; __ 71 m/s.

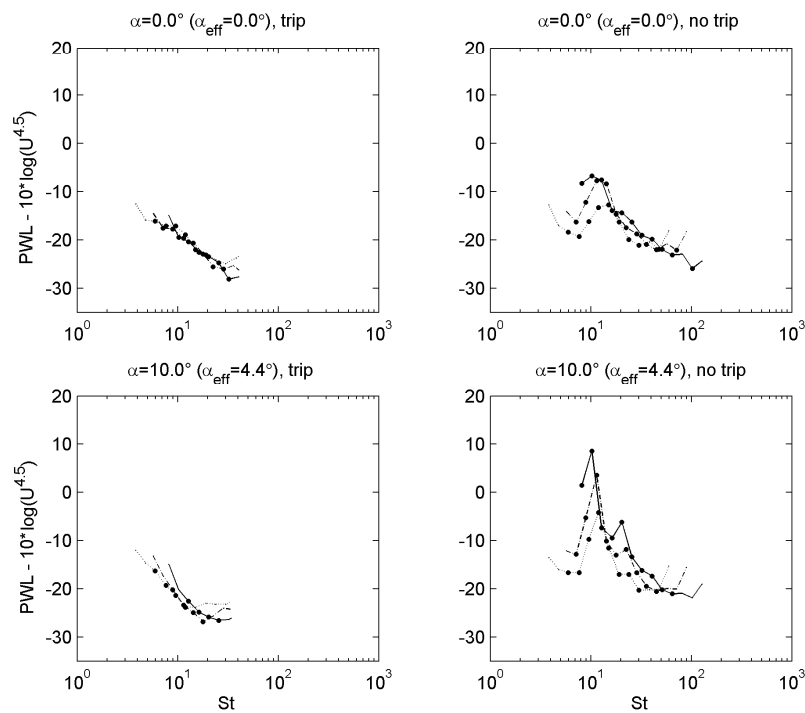


Figure 11: Normalized trailing edge noise spectra for S834 airfoil (compare to Figure 9): __ 22 m/s; _ _ 32 m/s; ... 48 m/s.

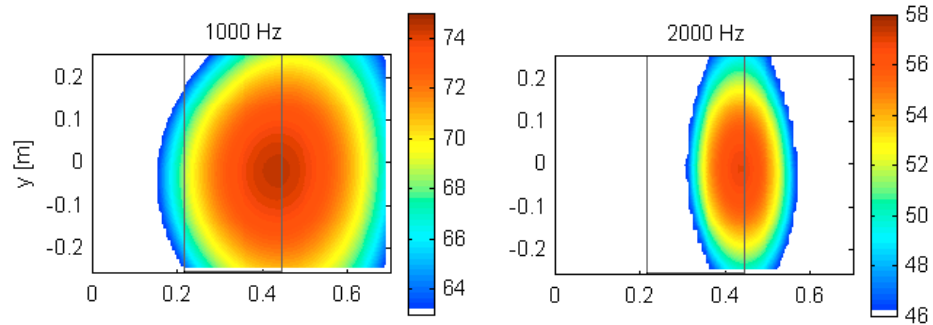


Figure 12: Acoustic source plots for the 1 and 2 kHz tones of the untripped S834 airfoil at 22 m/s and $\alpha=10^\circ$ (see Figure 9). Note the difference with the source plots for *broadband* trailing edge noise in Figure 3.

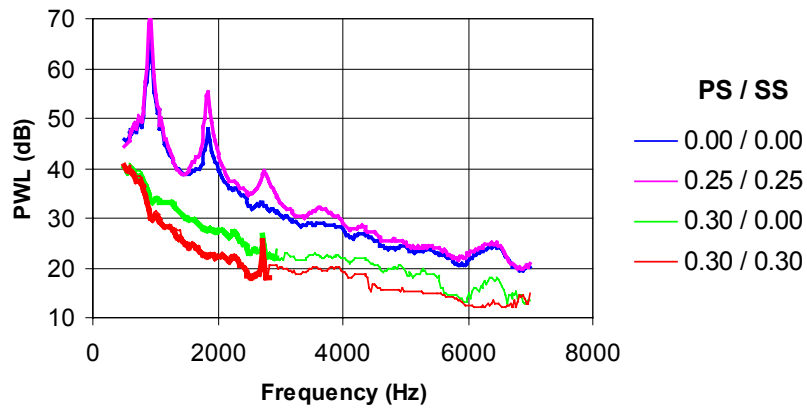


Figure 13: Dependence of trailing edge tones on trip thickness. Shown are the narrowband trailing edge noise spectra for the S834 airfoil at 22 m/s and $\alpha=10^\circ$, as a function of trip thickness on pressure side (PS) and suction side (SS). A thin line indicates that these spectral values are an upper limit for the actual trailing edge noise level. See also Figure 9 and Figure 12.

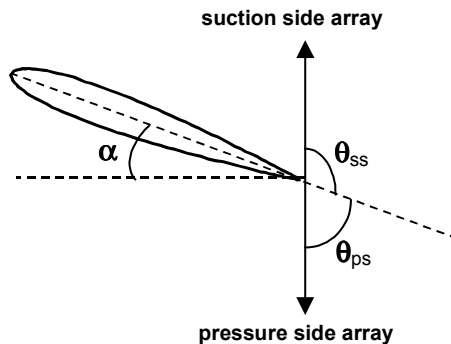


Figure 14: Illustration of difference in measured direction for pressure and suction side array, as a function of angle of attack.

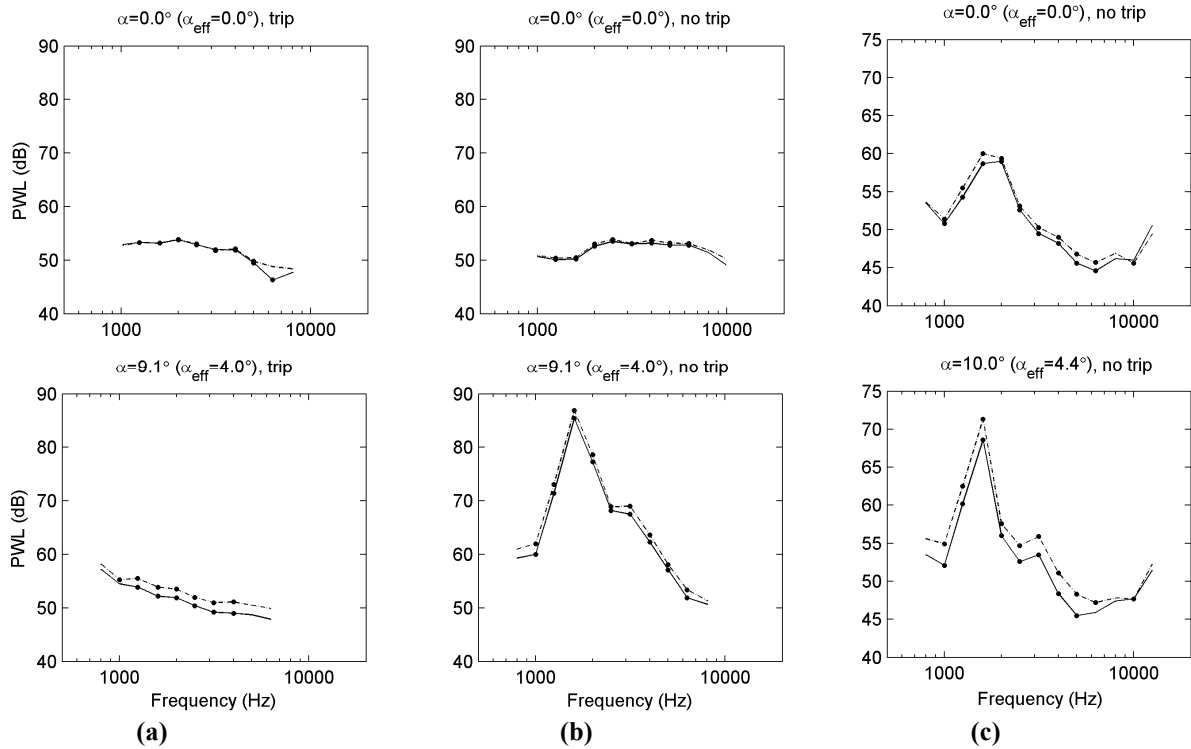


Figure 15: Directivity of trailing edge noise for NACA0012 airfoil at 40 m/s (a,b) and S834 airfoil at 32 m/s (c): — array on pressure side; - - array on suction side.

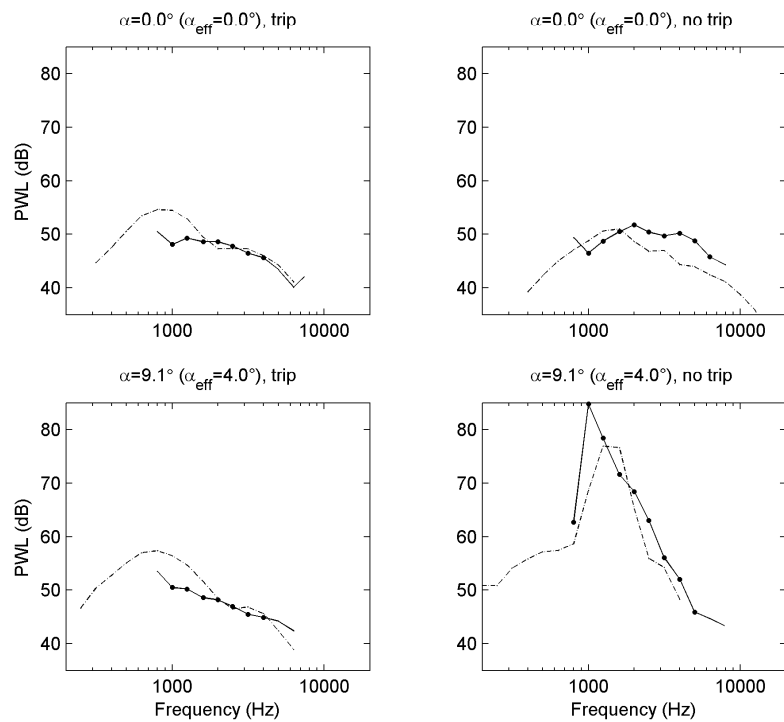


Figure 16: Comparison with benchmark data. Shown are trailing edge noise spectra of the NACA0012 airfoil at 32 m/s: — NLR data; - - NASA data.

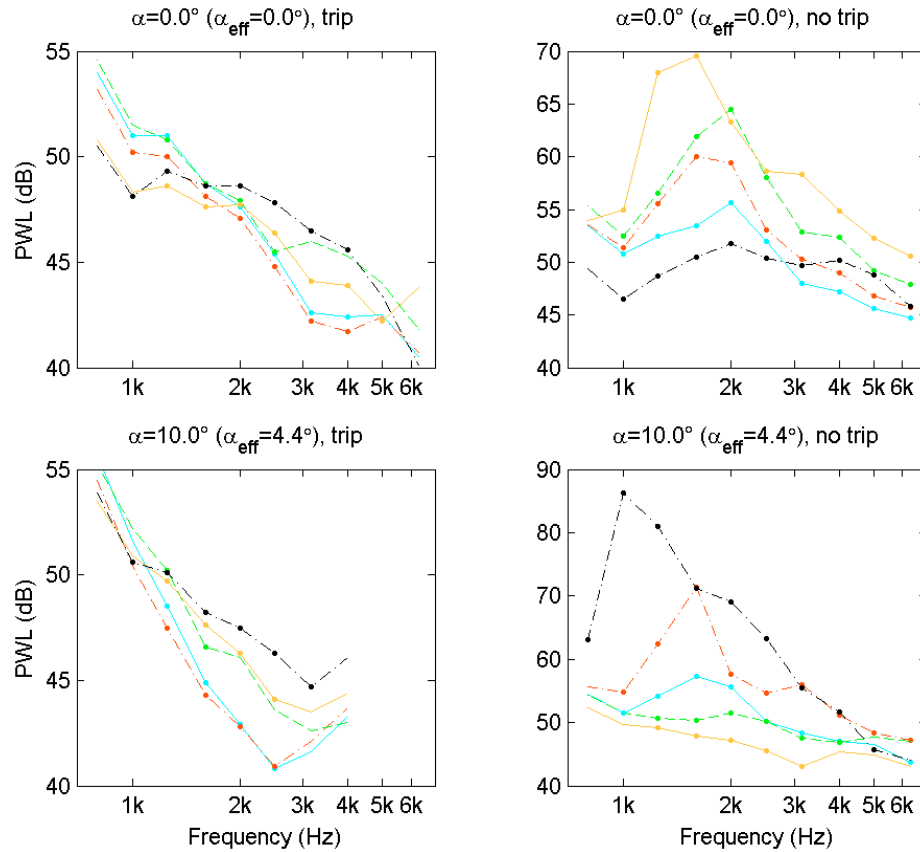


Figure 17: Comparison of trailing edge noise levels for different airfoils at 32 m/s: — S822; - - S834; ... SG 6043; - · - SD 2030; _ _ NACA0012. Note that the scales on the y-axis are different.

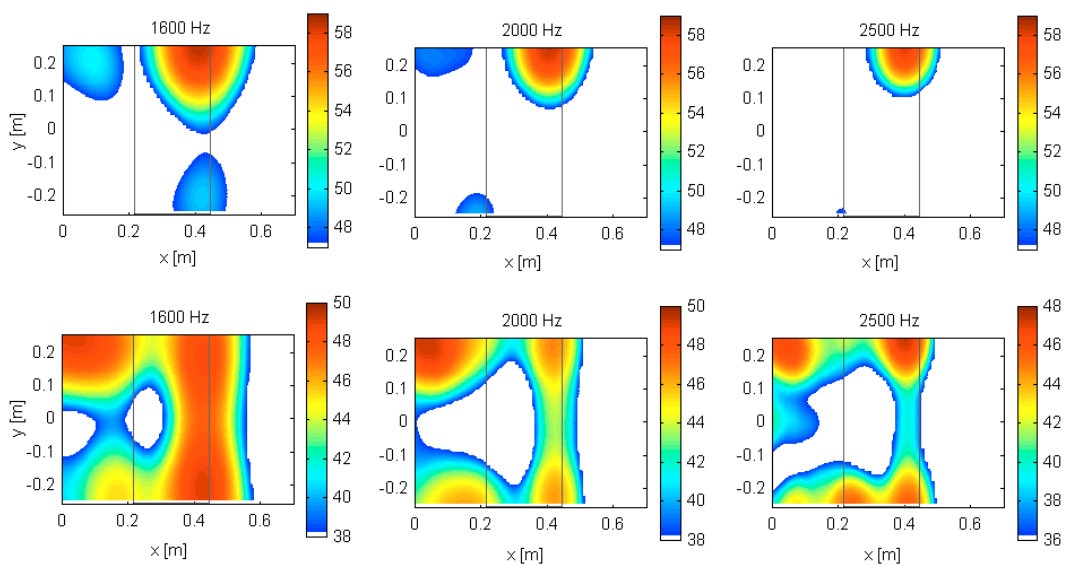


Figure 18: Reduction of extraneous noise sources through treatment with porous material. Without treatment (upper row), extraneous noise sources at the model-endplate junctions prevent the measurement of airfoil noise. After application of porous material at the junctions (lower row), the extraneous sources are drastically reduced and very low trailing edge noise levels can be detected. Note the different color scales.

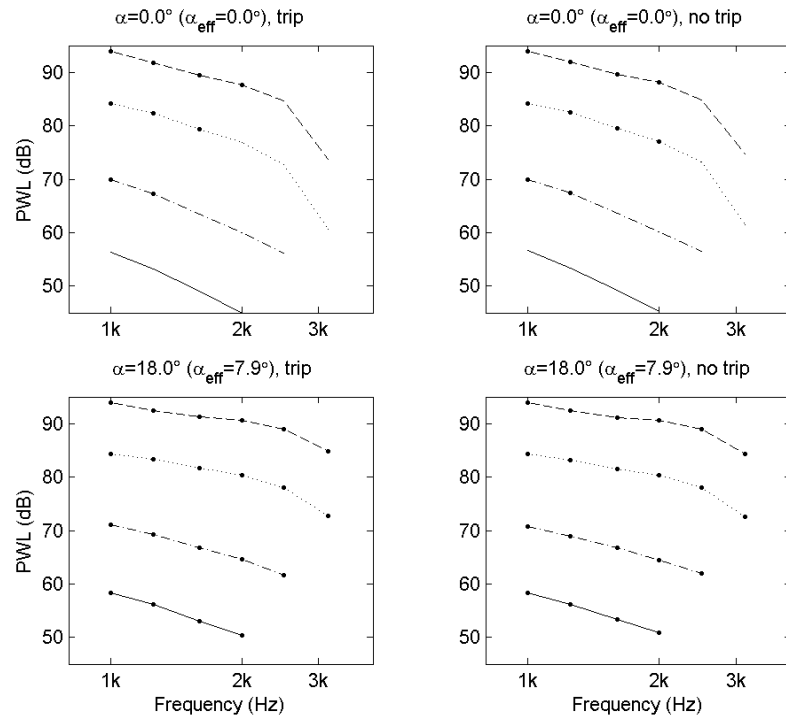


Figure 19: Inflow turbulence noise spectra for S822 airfoil: __ 22 m/s; _ _ 32 m/s; ... 48 m/s; __ 64 m/s.

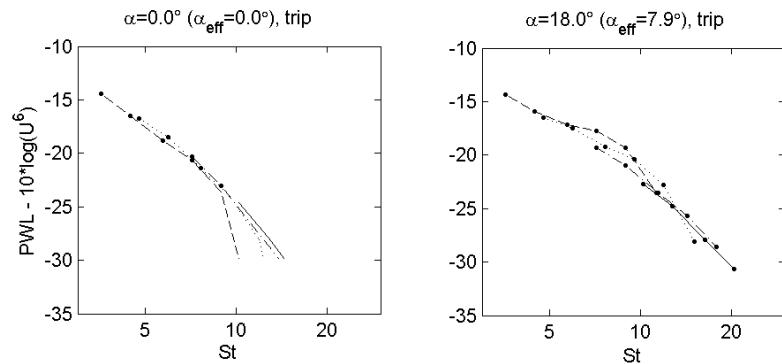


Figure 20: Normalized inflow turbulence noise spectra for S822 airfoil (compare to Figure 19): __ 22 m/s; _ _ 32 m/s; ... 48 m/s; __ 64 m/s.

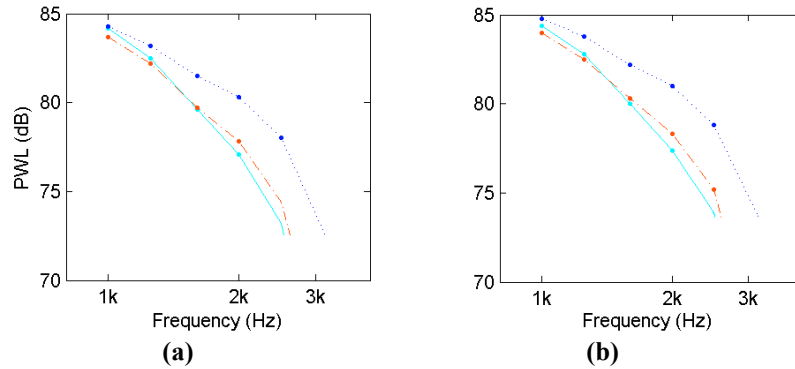


Figure 21: Dependence of inflow turbulence noise levels on angle of attack for S822 (a) and S834 (b) airfoils at 48 m/s: — $\alpha=0^\circ$; - - $\alpha=10^\circ$; ... $\alpha=18^\circ$.

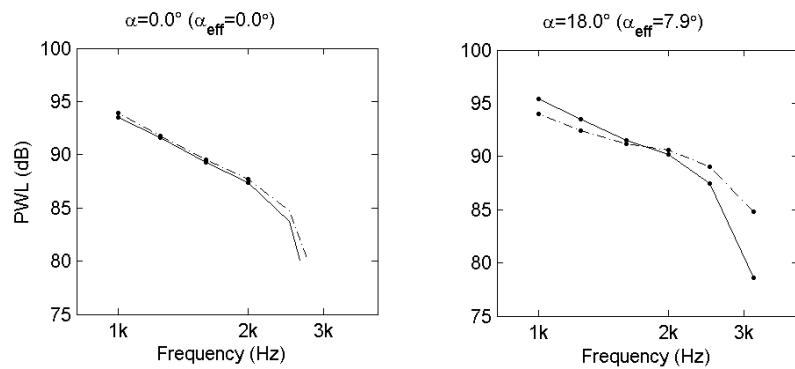


Figure 22: Directivity of inflow turbulence noise for S822 airfoil at 64 m/s: — array on pressure side; - - array on suction side.

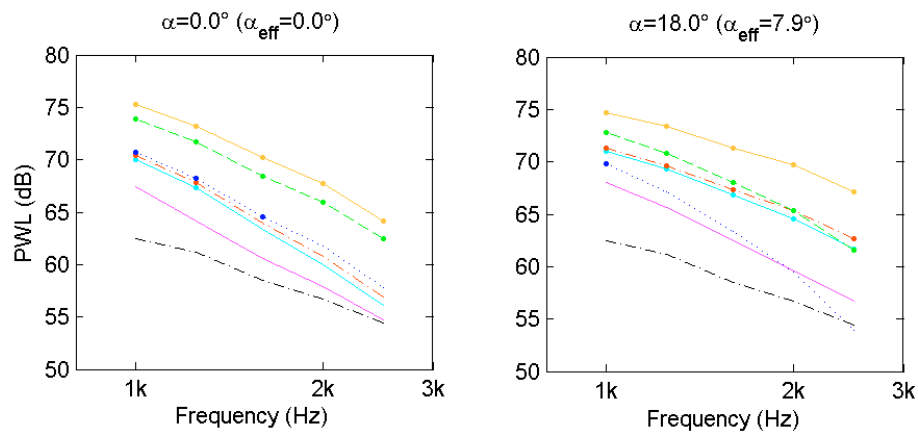


Figure 23: Comparison of inflow turbulence noise levels for different airfoils at 32 m/s: — S822; - - S834; ... FX 63-137; - - SG 6043 (no trip at $\alpha=18^\circ$); — SH 3055; — SD 2030; - - background noise (no model).